American Mineralogist, Volume 89, pages 1162–1175, 2004

Scanning Electron Microscopy investigations of laboratory-grown gas clathrate hydrates formed from melting ice, and comparison to natural hydrates

LAURA A. STERN,[1,*] STEPHEN H. KIRBY,[1] SUSAN CIRCONE,[1] AND WILLIAM B. DURHAM[2]

[1]U.S. Geological Survey, 345 Middlefield Road, MS 977, Menlo Park, California 94025, U.S.A.
[2]U.C. Lawrence Livermore National Laboratory, Livermore, California 94550, U.S.A.

ABSTRACT

Scanning electron microscopy (SEM) was used to investigate grain texture and pore structure development within various compositions of pure sI and sII gas hydrates synthesized in the laboratory, as well as in natural samples retrieved from marine (Gulf of Mexico) and permafrost (NW Canada) settings. Several samples of methane hydrate were also quenched after various extents of partial reaction for assessment of mid-synthesis textural progression. All laboratory-synthesized hydrates were grown under relatively high-temperature and high-pressure conditions from rounded ice grains with geometrically simple pore shapes, yet all resulting samples displayed extensive recrystallization with complex pore geometry. Growth fronts of mesoporous methane hydrate advancing into dense ice reactant were prevalent in those samples quenched after limited reaction below and at the ice point. As temperatures transgress the ice point, grain surfaces continue to develop a discrete "rind" of hydrate, typically 5 to 30 μm thick. The cores then commonly melt, with rind microfracturing allowing migration of the melt to adjacent grain boundaries where it also forms hydrate. As the reaction continues under progressively warmer conditions, the hydrate product anneals to form dense and relatively pore-free regions of hydrate grains, in which grain size is typically several tens of micrometers. The prevalence of hollow, spheroidal shells of hydrate, coupled with extensive redistribution of reactant and product phases throughout reaction, implies that a diffusion-controlled shrinking-core model is an inappropriate description of sustained hydrate growth from melting ice. Completion of reaction at peak synthesis conditions then produces exceptional faceting and euhedral crystal growth along exposed pore walls. Further recrystallization or regrowth can then accompany even short-term exposure of synthetic hydrates to natural ocean-floor conditions, such that the final textures may closely mimic those observed in natural samples of marine origin. Of particular note, both the mesoporous and highly faceted textures seen at different stages during synthetic hydrate growth were notably absent from all examined hydrates recovered from a natural marine-environment setting.

INTRODUCTION

As worldwide interest in gas hydrates—and their unusual behavior or properties—continues to grow, so too has the need for improved methods for careful determination of composition, grain morphology, and phase distribution in gas-hydrate-bearing samples of both laboratory and natural origin. Accurate sample characterization is critical to investigations of growth and formation processes as well as for reliable interpretation of physical property measurements. In particular, the presence and specific distribution of a secondary ice phase, i.e., unreacted ice, a dissociated ice product, or frozen-in pore water, can greatly influence the material characteristics of the bulk assemblage. Moreover, such alteration of naturally occurring hydrates during their transit to the surface may mask clues about their in situ state or growth processes.

A current challenge in gas hydrate research involves such evaluation of gas hydrate grain and pore structures, characteristics that are revealing guides to the physics and chemistry of hydrate growth as well as to the effects of environmental conditions or handling procedures. Pressurized optical cells have been used with demonstrated success to investigate growth habits of hydrate crystals from a wide range of environments (see Makogon 1997 or Sloan 1998 for overview; also Smelik and King 1997). Other microimaging techniques such as nuclear magnetic resonance (NMR; Moudrakovski et al. 1999; Mork et al. 2000), X-ray tomography (Mikami et al. 2000; Uchida et al. 2000; Freifeld et al. 2002), and magnetic resonance microimaging (MRM; Moudrakovski et al. 2002) have also proven to be elegant tools for non-invasive imaging of hydrate formation, distribution, or dissociation processes, as they offer excellent spatial and time resolution. NMR investigations by Moudrakovski et al. (1999), for example, yielded images that clearly show the interiors of ice grains (~200 μm) melting to liquid water at temperatures above the ice point, at moderate CH_4 pressures (6–12 MPa), with little or no collapse of the early formed outer hydrate shell. Using MRM, Moudrakovski et al. (2002) also followed the progression of CO_2 hydrate formed from melting ice grains, and successfully imaged the seemingly random distribution of nucleation and growth of hydrate grains within hydrate-encased liquid cores.

Scanning electron microscopy (SEM) offers yet another powerful technique for providing additional information on hydrate growth processes, due to its potential resolution, large depth of focus, and versatility in detection capabilities. Use of this technique for imaging gas hydrates has only recently been

* E-mail: lstern@usgs.gov

reported in the literature, however. Kuhs, Staykova, Klapproth, and coworkers (Kuhs et al. 2000; Staykova et al. 2002, 2003; Klapproth et al. 2003) used cryo-SEM techniques with excellent success to image and identify grain structures in CH_4, CH_4-N_2, CO_2, and Ar hydrates prepared from reaction of ice with gases or liquids, as well as to image natural gas hydrate from a marine setting (Suess et al. 2002). Their SEM investigations also revealed the remarkable development of highly mesoporous gas hydrate formed from ice at temperatures near the ice point. Our own group has also reported on SEM investigations of hydrates of both laboratory and natural origin, including pure and partially dissociated methane hydrate (Stern et al. 2003), compacted and deformed methane hydrate (Durham et al. 2003a), pure, porous CO_2 hydrate (Circone et al. 2003), and natural gas hydrate from the Gulf of Mexico (Stern and Kirby 2004).

When applying SEM to the study of any gas-hydrate-bearing material, natural or synthetic, numerous technical challenges must be overcome: (1) avoiding condensation of atmospheric water on samples during cold transfer, (2) coating the samples if necessary with an electrically conductive layer without introducing heat or damage to the sample surface, (3) maintaining the hydrate sample material at conditions that avoid spontaneous decomposition or significant sublimation under vacuum, and (4) either avoiding electron beam damage of the imaging area or learning to properly identify it when it occurs. Distinguishing handling-induced surface artifacts from the intrinsic sample surface morphology can be difficult, as well as distinguishing hydrate from ice. For the specific study of natural gas hydrates, these challenges are amplified by such additional unknowns as the complex in situ environmental conditions controlling the original growth textures, or the effects of subsequent recrystallization, annealing, secondary growth, dissociation, dissolution, or chemical exchange processes. The indeterminate extent of sample damage or alteration incurred during retrieval and subsequent storage or handling of the hydrate presents additional unknowns. Hence, without a wider sampling archive and additional experience in assessing these issues, most interpretations of SEM images of natural gas hydrates should be regarded as somewhat speculative. Nonetheless, some useful information about grain structure, pore characteristics, phase composition, and phase distribution may still be obtained if the natural hydrates can be compared to other materials that have known compositions as well as known formation and/or processing histories.

Here, we apply SEM techniques to observe grain and pore structure development associated with gas hydrate formation from reaction of a hydrate-forming gas or liquid with melting ice under static and constant-volume conditions. We first show images from specific tests performed on synthetic hydrates to investigate the inherent effects of cryo-SEM preparation and/or imaging procedures. These images are intended to alert the reader or SEM user to possible surface damage or alteration that can be confused with original sample growth textures or surface morphology. We then look at laboratory-synthesized gas hydrates of known purity, composition, and pressure-temperature (*P-T*) processing histories, and present images conveying the range and variety of textures observed at various extents of reaction. We then image synthetic gas hydrate samples used in increasingly complex laboratory and ocean-floor experiments, and compare the observed features to those developed within natural gas hydrate nodules recovered from both marine and permafrost settings. Lastly, we discuss the implications for the reaction process in light of our own previous results as well as those of others.

Experimental method

Laboratory synthesis of gas hydrates

Large-volume (30–50 g) samples of pure, polycrystalline, structure I (sI) and structure II (sII) gas hydrates, and various hydrate + sediment mixtures, were synthesized by previously published methods, listed below by composition. Briefly, synthesis involves the warming and static conversion of a measured mass of small grains (<250 μm) of H_2O ice to gas hydrate in an atmosphere of pressurized hydrate-forming gas or liquid. The ice + gas reactants were introduced at 250 K and elevated pressure, then warmed to peak synthesis conditions deep within the hydrate's stability field and well above the H_2O ice melting point. Figure 1a depicts synthesis conditions specific to methane hydrate formation. One to four thermocouples located within the sample (or companion sample), as well as a thermocouple and RTD probe in the surrounding fluid bath, monitored thermal conditions during reaction (Fig. 1b; also see Fig. 1 in Circone et al. 2004, this volume) and take-down procedures. Pressure transducers monitored gas pressure in the sample chamber. A multi-hour hold at peak conditions, or in some cases repeated cycling of the sample temperature through the ice point, produced complete reaction such that the ice reactant was fully consumed, with only the gas reactant (or liquid, as in the case of propane or CO_2) remaining in excess. Samples were then cooled to 250 K while still under pressure. Complete reaction was inferred by the lack of a freezing anomaly in the synthesis record, and by the extent of gas uptake in relation to the mass of the initial ice pack. Samples were then rapidly quenched to 77 K for subsequent investigation. Pressure was released after the central sample thermocouple showed that the interior was substantially colder than the 0.1 MPa dissociation temperature. The resulting hydrate is a white, finely granular but cohesive material with typically 30% intergranular porosity.

This general technique, modified for each specific gas hydrate composition in accordance with that hydrate's equilibrium phase relations, was used to produce samples of pure sI methane hydrate with "as-grown" composition $CH_4 \cdot 5.9H_2O$ (Stern et al. 1996, 2000; Circone et al. 2001); sI CO_2 hydrate of composition $CO_2 \cdot 5.7H_2O$ (Circone et al. 2003); sII methane-ethane hydrate made from a source gas of $0.9CH_4 + 0.1C_2H_6$ and resulting in hydrate composition $(0.82CH_4 + 0.18C_2H_6) \cdot 5.67H_2O$ (Stern et al. 2003; Helgerud et al. 2003; Rawn et al. 2002); sII propane hydrate of nominal composition $C_3H_8 \cdot 17H_2O$ (Rawn et al. 2003); and variously layered or mixed methane hydrate + sediment mixtures (Stern et al. 2000). X-ray diffraction data, ultrasonic measurements, and/or gas-collection measurements that demonstrate the purity of the resulting hydrate are shown in these previously published papers. Three additional samples of methane hydrate were also quenched at specific mid-synthesis intervals for detailed observation of reaction progression as reactants warmed above the ice point (Fig. 1, points A–C), and for comparison to samples that achieved complete reaction following the isothermal hold at peak synthesis conditions (Fig. 1, point D). For quenching of methane-bearing hydrates, sample vessels were plunged into liquid nitrogen and depressurized to 0.1 MPa after the sample's interior cooled below 150 K. Quenching of CO_2 and propane hydrates involved additional procedures to avoid freezing a solid CO_2 or propane phase into the final material (see Circone et al. 2003; Rawn et al. 2003).

Four samples of methane hydrate were also synthesized for investigation of hydrate stability and textural changes produced by exposure to natural ocean-floor conditions. Two were maintained as "as-grown" porous methane hydrate, and two others were subjected to hydrostatic compaction that reduced porosity from 30% to less than 3% porosity (Durham et al. 2003a). Samples were then transported under methane pressure to a seafloor test site at 1030 m water depth, then opened and exposed to that environment for observation and measurement (see Rehder et al. 2004 and Stern et al. 2002 for further technical description). Those samples that did not undergo complete dissolution after 27 hours were successfully recovered and returned to the laboratory for SEM analysis.

Finally, we examined several natural gas hydrate specimens collected from both marine and permafrost environments. The marine samples were retrieved by piston coring in 2002 by the *RSV Marion Dufresne*, from a 1032 m depth site in the Mississippi Canyon, Gulf of Mexico (Winters et al. 2004). Permafrost hydrates were recovered by drillcore from 1000 ±150 m depth at the Mallik site, Mackenzie

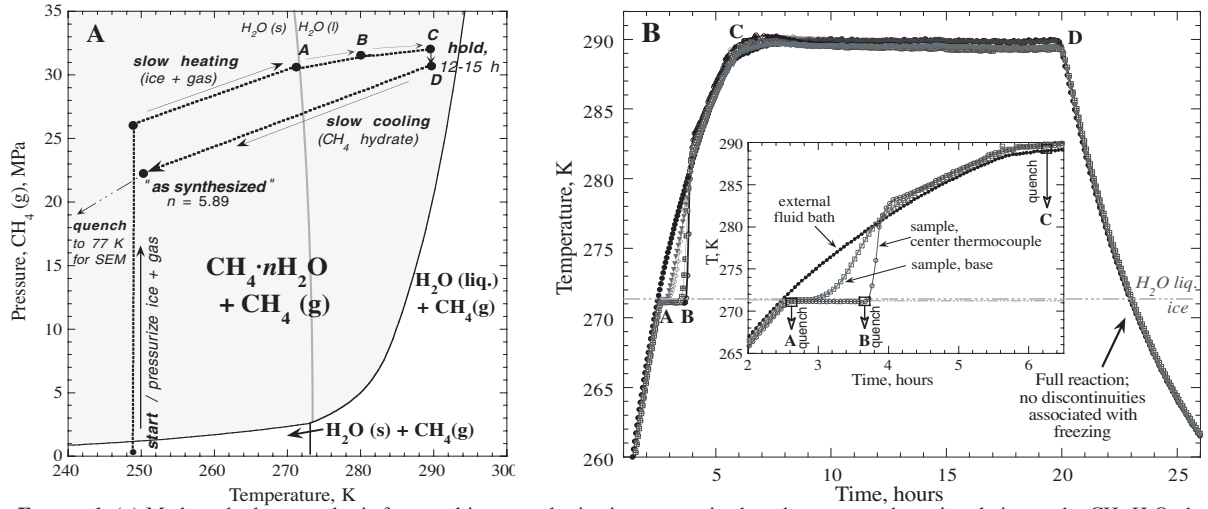

FIGURE 1. (**a**) Methane hydrate synthesis from melting granular ice in a pressurized methane atmosphere, in relation to the CH_4-H_2O phase diagram. Shaded region shows the methane hydrate equilibrium stability field. Black dotted lines trace schematically the general reaction path during synthesis (Stern et al. 1996, 2000). The metastable extension of the H_2O melting curve is shown by the solid grey curve. Points A, B, and C show the extents of partial reaction for samples that were quenched for observation of mid-synthesis growth textures, and for comparison to the grain morphology developed within fully reacted samples (point D). (**b**) Temperature-time profile during hydrate formation. The thermal state of the sample as it warms through the H_2O melting point is expanded in the inset. Solid black circles denote the external bath temperature, and open symbols track internal sample thermocouples. Points A-D correspond to those shown in (**a**). Buffering of the sample thermocouples near the H_2O melting point indicates that a large fraction of ice melting occurs over this 1.2 h stage (see also Circone et al. 2003). We previously speculated that the measured *P-T* anomaly that accompanies this stage was not sufficient to account for full melting of the unreacted ice (Stern et al. 1996, 2000). Recent determination of the high strength (Durham et al. 2003a, 2003b) and low thermal conductivity (Waite et al. 2002a, 2002b) of methane hydrate, however, now shows that it has material characteristics different from those previously predicted. These properties may serve to partially mask the full *P-T* melting signature of unreacted ice cores. See text for further discussion.

Delta, NW Canada (Dallimore and Collett 2004). All samples arrived by air freight in liquid-nitrogen-cooled vapor shippers. The marine hydrates were transferred upon arrival to dry, deep-freezer storage at 180 K and 0.1 MPa air pressure. The permafrost hydrates remained in LN storage.

SEM preparation and imaging

Prior to imaging, each sample was immersed in liquid nitrogen while a small section of hydrate, typically ~0.75 × 0.75 × 0.5 cm, was cleaved and attached to a brass sample holder. The dished holder clamps the sample by contact points at its sides, and has a thin floor to maintain close thermal contact with the stage on which it is mounted. Samples were then quickly transferred to a sample stage within an evacuated and pre-chilled (below 100 K) Gatan Alto 2100 cryo-preparation and coating station, which was in turn attached to a LEO 982 field emission SEM. While still in the preparation chamber, the section was again fractured with a cold blade to produce fresh surfaces for imaging that were not contaminated by surface condensation. The samples were in some instances coated with AuPd for 60 s using a non-heat-emitting sputter head. This procedure, with working distance and voltage set specifically for low-temperature maintenance, produces "islands" of AuPd of ~1 nm thickness, i.e., well below the imaging resolution of all gas hydrates examined here. Companion samples were also imaged uncoated to ensure that surface topology was not altered by the coating process (Fig. 2). The samples

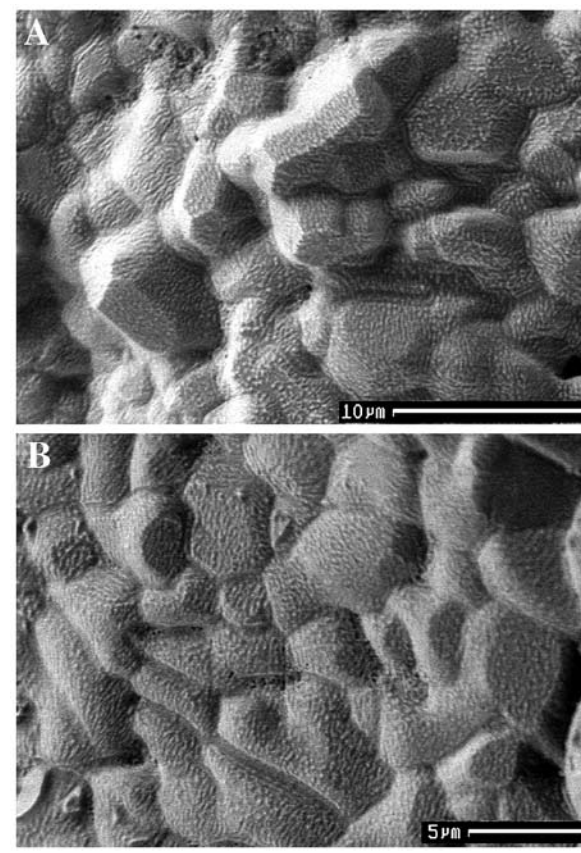

FIGURE 2. Coating test on synthetic methane hydrate. This sample was fractured at ~100 K under vacuum, initially imaged uncoated at 2 kV and 100 K (**a**), then re-inserted in the cryo-preparation chamber and coated with AuPd for 120 seconds at 100 K. The same general area of the sample was then re-imaged at the initial test conditions (**b**). Comparing (**a**) with (**b**) indicates that low-temperature coating causes no apparent damage or alteration to the sample surface. For porous and loosely granular hydrates, coating helps alleviate electrical charging and "flares" on the sample surface that can degrade image quality.

were then inserted directly through the back of the preparation chamber and on to an auxiliary cryo-imaging stage in the SEM column. Sample temperature was continuously monitored by thermocouples, one embedded just below the surface of the preparation-chamber sample stage, and one placed identically within the SEM-chamber sample stage. Imaging was conducted at temperatures below 105 K and vacuum below 10^{-5} mbar, using low voltage (≤2 kV) to minimize sample alteration or beam damage of the sample surface (Figs. 3 and 4). Several imaged areas were re-examined later in each session to monitor changes in surface topology over time (Figs. 4c and 4d), a procedure we routinely use during SEM imaging of any hydrate- or ice-bearing materials.

Phase identification, in certain cases, remains problematic. Port requirements necessitate the removal of the back-scattered electron detector when the

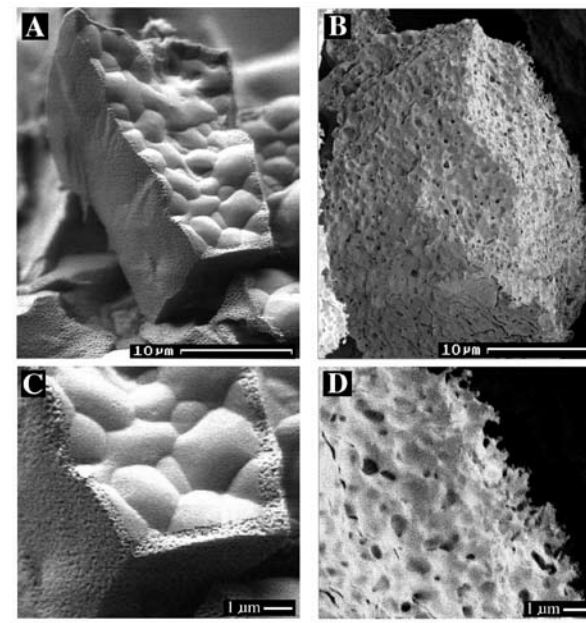

➜

FIGURE 3. Surface damage by thermally induced dissociation. (**a**) This methane hydrate fragment along the fresh fracture surface shows the effects of surface damage (outer meso- or nano-porous "rind") after delayed transfer into the cryo-preparation station. (**b**) This grain was originally fully dense methane hydrate that was intentionally subjected to brief warming (~12 min) in the SEM chamber from 140 to 195 K to induce surface dissociation. The sample was then rapidly cooled to preserve the dissociation texture for imaging. Images (**c**) and (**d**) are enlargements from (**a**) and (**b**), respectively, detailing the characteristic porous texture of ice as it occurs as a low-temperature hydrate dissociation byproduct. Distinguishing porous dissociation textures from similarly appearing growth textures (Fig. 5) can often be difficult without knowledge of the sample history. The fracture through the cavity fragment in (**a**) also shows that this hydrate is densely crystalline on the sample interior.

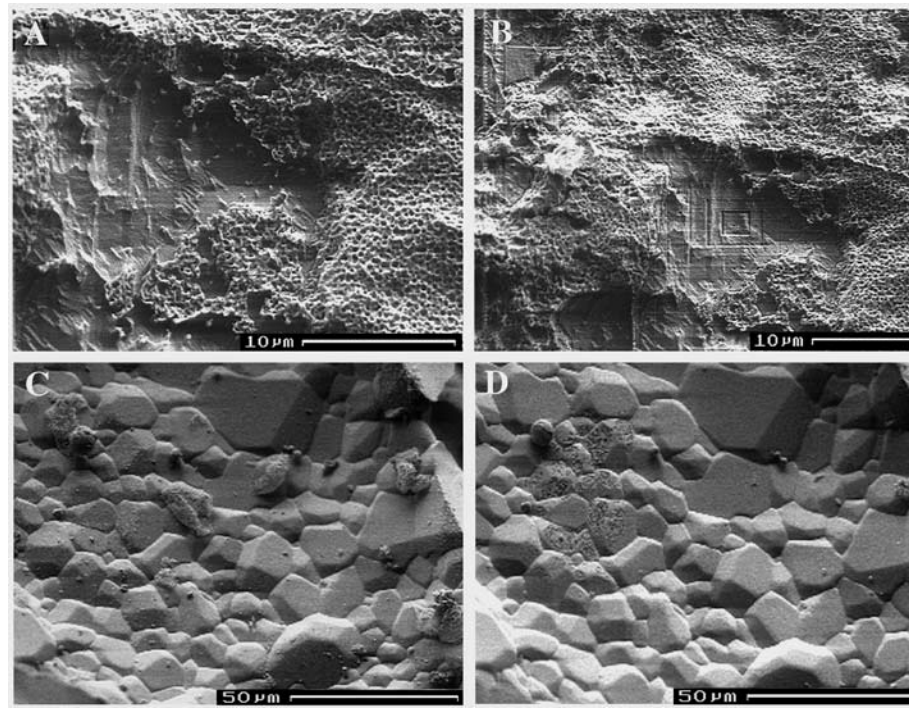

FIGURE 4. Surface damage due to combined thermal and beam effects (**a** and **b**) and vacuum exposure (**c** and **d**) incurred during SEM procedures. Images (**a**) and (**b**) show a fully compacted sample of sII methane-ethane hydrate that underwent minor surface dissociation during protracted loading procedures. Energy dispersive X-ray (EDX) scans confirmed that the smooth, dense material in the background is hydrate, and the thin, porous, surface layer is ice (see text for further discussion; also compare to Fig. 3). This sII hydrate was fragile under the beam, incurring rectangular "burn" marks during routine focusing procedures. Image (**a**) was taken by focusing on a region adjacent to the field of view, then relocating to the current area for imaging. The beam was then refocused inside the field of view before taking image (**b**). In (**b**), five rectangular "rastering" patterns can be seen on the hydrate surface (prominent in upper-left and central sections), each produced as the 2.0 or 1.5 kV beam was held for five-second intervals before retracting to a different focal distance. The dissociated ice product along the sample surface shows no similar response to the beam. Although image (**b**) appears to show that the porous surface layer developed after (and "on top" of) the burn marks, comparison to (**a**) proves otherwise, and also demonstrates the different responses of these two phases to the beam. Images (**c**) and (**d**) show the same area before and after vacuum exposure on lab-synthesized CO_2 hydrate over a 165 min time interval. Most of the small pieces of surface ice (condensate) in (**c**) eventually sublimated and do not appear in (**d**). Regions of hydrate surface pitting have also developed during the vacuum exposure, as exhibited in the upper left quadrant of (**d**). Photo sequences (**a-b**) and (**c-d**) underscore the need for periodic return to previously viewed sections of samples to monitor topological changes and to avoid confusion of SEM-induced morphological artifacts with original sample textures.

cryosystem is in use. Hydrate often can be distinguished from ice using X-ray (EDX) capabilities, but resolution is limited by the long focal distance (~15 mm) needed for this technique, combined with the low accelerating voltage needed to minimize sample damage. Carbon peaks were small but identifiable by EDX in dense grains of methane or methane-ethane hydrate, but more difficult to resolve in highly porous, uneven, or partially dissociated samples. Surface morphology, supplemented with EDX measurements and in some cases beam damage assessment, remains our most useful tool for phase identification of individual grains during a given SEM session. Powder X-ray diffraction was usually used for bulk-sample phase identification.

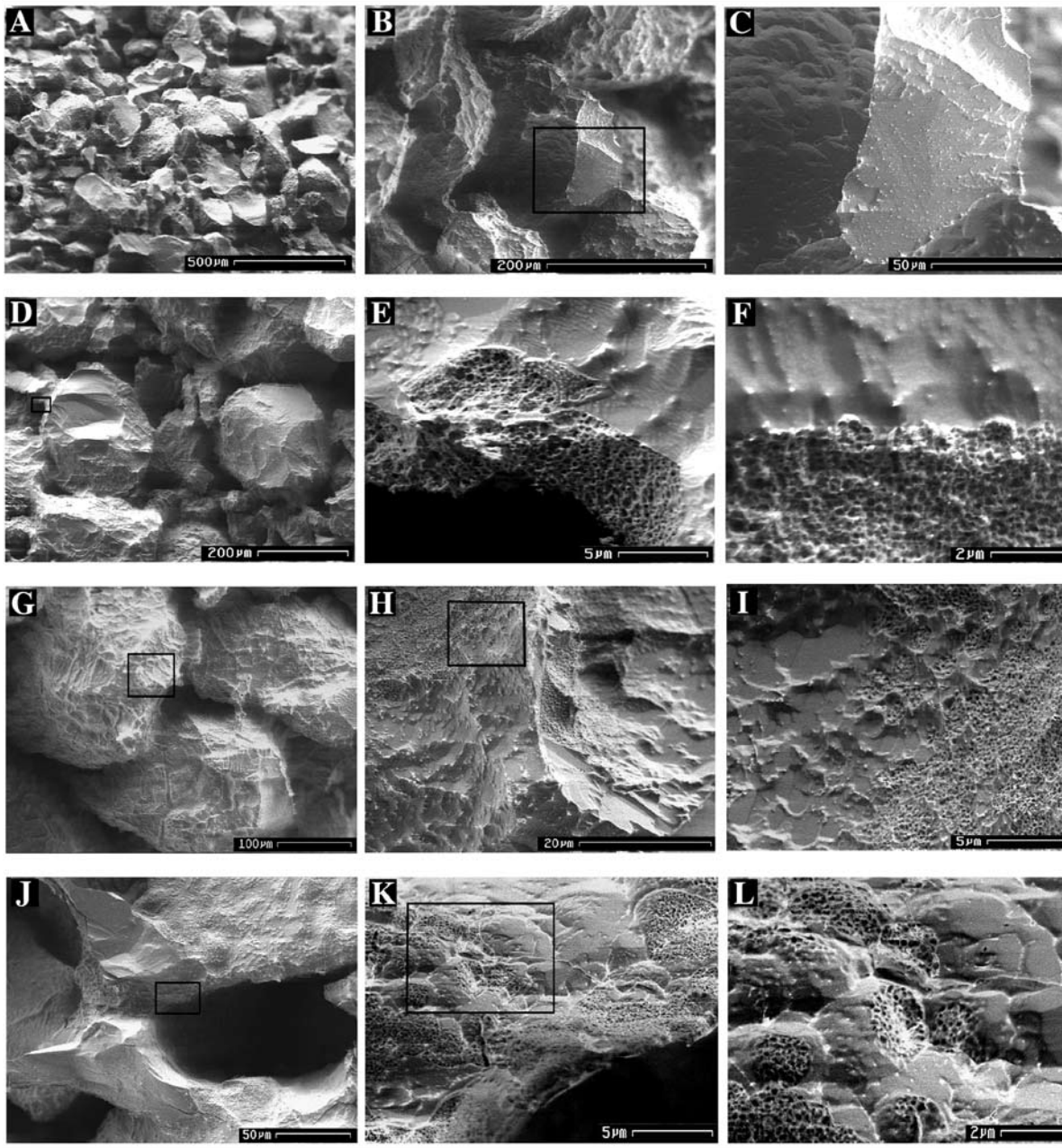

FIGURE 5. Early-stage growth of methane hydrate from melting ice near the ice point, from points A to B in Figure 1b. (**a**–**c**) show low to high magnification images of a fresh fracture through the center of a sample quenched immediately upon reaching the ice point (Fig. 1b, point A). Minimal reaction precedes this stage, and ice "seeds" retain their uniformly dense texture. (**d**–**f**) show the basal section of the same sample, from an area that was at the ice melting point for 0.3 hours. Reaction and growth of highly mesoporous methane hydrate is visible along nearly all exposed ice-grain surfaces, growing inward along crystallographically determined fronts (**e**) or in more irregular and "clustered" progression of ~ **1** μm subgrains (**f**). (**g**–**i**) and (**j**–**l**) show upper and central sections, respectively, of a sample quenched at the end of the ice-point "buffer" stage (Fig. 1b, point B). (**g**–**i**) show advancement of mesoporous hydrate and concurrent development of several-micrometer-sized domains. Samples tend to fracture through the weaker ice phase, sometimes obscuring the apparent geometrical arrangement of phases. (**j**–**l**) show the onset of annealing and "densification" of the hydrate phase. Incipient crystal-face development is seen in (**l**). Outlined insets in (**b**), (**d**), (**g**), (**h**), (**j**), and (**k**) are expanded in the image to the right.

RESULTS

Surface artifacts produced during cryo-SEM procedures

Several tests were conducted on various gas hydrate test specimens to identify possible surface damage or alteration effects that can be incurred during routine SEM preparation and imaging procedures (Figs. 2–4). The results of one experiment investigating potential coating effects are shown in Figure 2. Side-by-side comparison of uncoated vs. coated methane hydrate demonstrates that the observed fine-scale surface features are not produced by coating procedures or the AuPd coat itself. Other tests were undertaken to investigate the texture and surface appearance produced by low-temperature (~195 K) dissociation of hydrate to ice. Such low-temperature dissociation always produced a markedly sponge-like or aerated texture (Fig. 3). At warmer temperatures in the "premelting" zone of ice (~260–273 K), where mobility of H_2O molecules along ice surfaces is high, dissociated surfaces appear dense, with low surface area features (Fig. 4 in Stern et al. 2003, for example). These results underscore the importance of such image comparisons and tests; distinguishing low-temperature dissociation from certain growth textures (compare Figs. 3, 4, and 5), or distinguishing dissociation caused by improper analytical methods from that incurred previously, can be challenging without full knowledge of the sample's history.

Other examples of sample instability under the beam, or during prolonged vacuum exposure, are shown in Figure 4. Different compositions or structures of hydrate were found to respond differently to SEM environmental conditions, reinforcing the need during each imaging session to revisit previously viewed areas for damage assessment. Structure II methane-ethane hydrate was found to be more fragile and prone to changes under the beam than sI methane hydrate, sI CO_2 hydrate, or sII propane hydrate, even though it is stable over a significantly wider range of *P-T* conditions than pure methane hydrate. All gas hydrates were more susceptible to beam and/or vacuum damage than H_2O ice, even at temperatures below 100 K. Time-lapse imaging proved critical for establishing whether surfaces had sublimated to reveal a different texture below, or if surface damage produced regions of hydrate breakdown (Figs. 4c and 4d).

Laboratory-synthesized gas hydrates

Figures 5, 6, and 7 show the textural progression and grain structure development accompanying methane hydrate formation by the procedure described above and shown in Figure 1. Figures 5 and 6 show samples that were quenched at specific extents of partial reaction (points A, B, and C shown in Fig. 1). Figure 5 shows that methane hydrate initially develops as a highly mesoporous material that nucleates at exposed ice surfaces, forming sharply defined boundaries with the dense ice reactant. Figure 6 illustrates the progressive annealing and well-developed crystal faceting that then accompanies further reaction with increasing *P-T* conditions. Figure 6 also shows strong evidence that after the hydrate forms an external "rind" along the melting ice grain surfaces, the grain interiors empty, presumably as melt migrates out of the hydrate encasement.

The resulting "as-grown" methane hydrate is shown in Figure 7 (corresponding to the product cooled and quenched from point D in Fig. 1). Although the material maintains a remnant texture reflecting the original seed ice pack (Fig. 7a), higher magnification reveals substantial recrystallization and redistribution of the solid phase, such that clusters or "domains" of fully dense grains, typically several tens of micrometers in grain size, dominate the final product (Fig. 7b). In fully reacted samples, the rind or "hollow shell" structures are sometimes retained near the base of the samples (Figs. 7c and 7d), or in samples that formed from a dense ice pack. There is no obvious indication in any of the samples that the hydrate encasements undergo massive failure

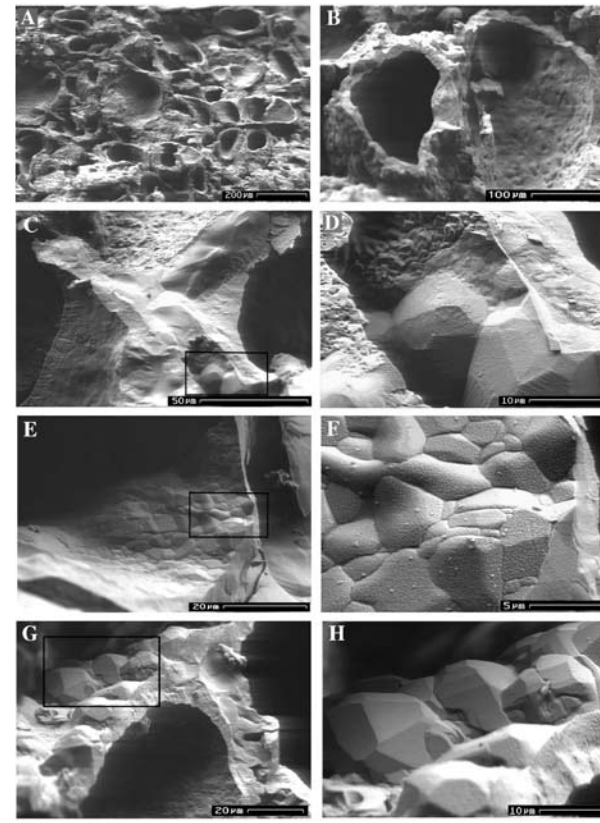

FIGURE 6. Late-stage recrystallization and annealing of methane hydrate at peak synthesis conditions, from points B to C in Figure 1b. After initial growth as a mesoporous material (Fig. 5), methane hydrate undergoes significant recrystallization and annealing with increasing temperature. Concurrent is the apparent melting of at least many of the cores of original ice grains. (**a**) and (**b**) show fresh fractures through a section of sample quenched at the end of the ice-melting "buffer" stage (base of sample B shown in Fig. 1b inset). The "shells" of hydrate, typically 5-20 μm thick, presumably form as liquid water extrudes or is expelled from the grain interior after initial hydrate formation along the grain exterior. This melt forms hydrate in nearby grain junctions (visible in **c** and magnified in the upper-left quadrant of **d**), rather than pooling, and contributes to the general competence of the final material. (**c**–**d**), (**e**–**f**), and (**g**–**h**) show methane hydrate from a sample quenched just upon reaching peak synthesis conditions (sample C in Fig. 1b inset). These sequences show annealing of the hydrate "shell" (**c**, **d**), the inner cavity lining (**e**–**f**), and the outer shell texture (**g**–**h**) into progressively larger and denser grains of hydrate that dominate the final "as-synthesized" material (compare to Fig. 7).

associated with core melting; instead, near-spherical morphology is typically maintained (Figs. 6a, 6b, 7c, and 7d). A somewhat less porous material is also commonly found in grain junctions (Fig. 6d, upper left quadrant). We presume that this material formed from the extruded melt phase from nearby or adjacent grains, an interpretation supported by our previous work that showed that the melt phase does not macroscopically segregate and pool in samples made from 250 μm ice grains under high *P-T* synthesis conditions (Stern et al. 1998b, 2000). Complete reaction with a subsequent multi-hour hold at peak synthesis conditions then produces exceptional faceting and crystal-face development along exposed pore walls or other free surfaces (Figs. 7e–h).

Carbon dioxide hydrate and pure propane hydrate grown from melting ice at *P-T* conditions above the ice point showed similar, but not identical, features (Fig. 8). Both show final grain and pore structures comparable to those in methane hydrate. Fracture surfaces expose hollow cavities lined by thin, dense, hydrate walls, creating a final texture reflective of early outer-surface reaction followed by subsequent melting of the unreacted ice-grain cores. Euhedral crystal growth forms along some cavity walls or exposed surfaces (Figs. 8a and 8c), but is less extensive than in methane hydrate. We speculate that the inability to access high *P-T* conditions during synthesis of CO_2 or propane hydrate (relative to methane hydrate), due to the lower-temperature limits imposed by their phase equilibria, is partially responsible for the poorer crystal face development.

Methane hydrate + sand mixtures also show evidence for extensive recrystallization in their final textures, such that hydrate forms both a coating and a loose "cement" between sand grains (Figs. 9a and 9b). Hollow cavities from melted ice cores are less prevalent in these samples than in pure methane hydrate. The higher thermal conductivity and diffusivity of the sand grains increases the rate of heat flow to sample interiors during synthesis, and may serve to increase the mobility of H_2O molecules and

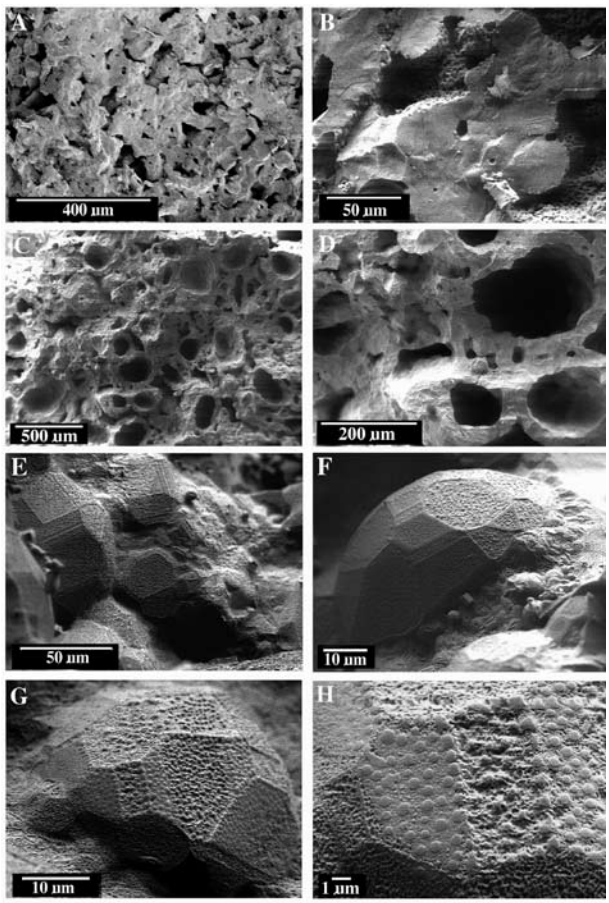

FIGURE 7. SEM micrographs of pure, fully reacted methane hydrate, formed as shown in Figure 1. (**a**) Low magnification shows the granular-but-cohesive texture that is quite different from the simple spherical grain shapes and geometrically simple pore shapes of the original ice pack. Gross particle morphology is commonly maintained, however. (**b**) Higher magnification reveals that considerable recrystallization takes place during full reaction, producing a framework of domains of dense, fine-grained hydrate with typical grain size of several to 10's of μms. (**c** and **d**) In some samples formed from a dense initial ice pack, or in other hydrate systems that do not permit synthesis at highly overdriven *P-T* conditions, hollow "shells" of hydrate remain prevalent within certain sections of samples (see also Figs. 6 and 8). (**e** and **f**) Features imaged along pore walls vary from sample to sample, but many of the "bumps" seen at lower magnification are small hydrate crystals with characteristic cubic-crystal facets. (**g** and **h**) Highest magnification reveals tiny dome-shaped structures on these crystal facets that we interpret as original growth structures. All samples shown here were prepared, coated, and imaged under high vacuum conditions at temperatures near 105 K, as described in the text.

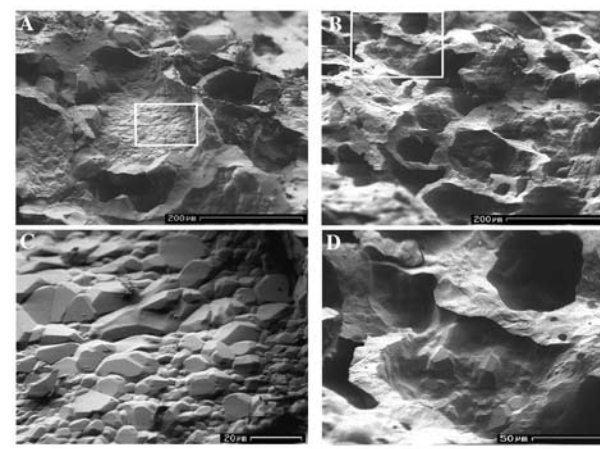

FIGURE 8. Textural development in other gas hydrates formed from melting ice under elevated *P-T* conditions, here using liquid hydrate-forming components. (**a**) Fresh fracture surface through pure, sI CO_2 deuterohydrate ($CO_2 \cdot 5.8D_2O$), grown by methods detailed in Circone et al. (2003). (**b**) Pure, sII propane hydrate ($C_3H_6 \cdot 13H_2O$) grown by methods discussed in text and in Rawn et al. (2003). Both low-resolution images show extensive recrystallization around remnant "shells", similar to those shown in Figures 6 and 7c–d. The common development of fully formed hydrate crystals as seen in methane hydrate grown at 290 K and 30 MPa (Figs. 7e–h) is less prevalent in CO_2 and propane hydrate, however, likely due to the limits placed on synthesis temperatures by the limits of hydrate stability. Nevertheless, faceted cavity walls are pervasive in all hydrates grown to-date from melting ice at temperatures above the ice point. Enlargements of outlined areas in (**a**) and (**b**) are shown in (**c**) and (**d**), respectively.

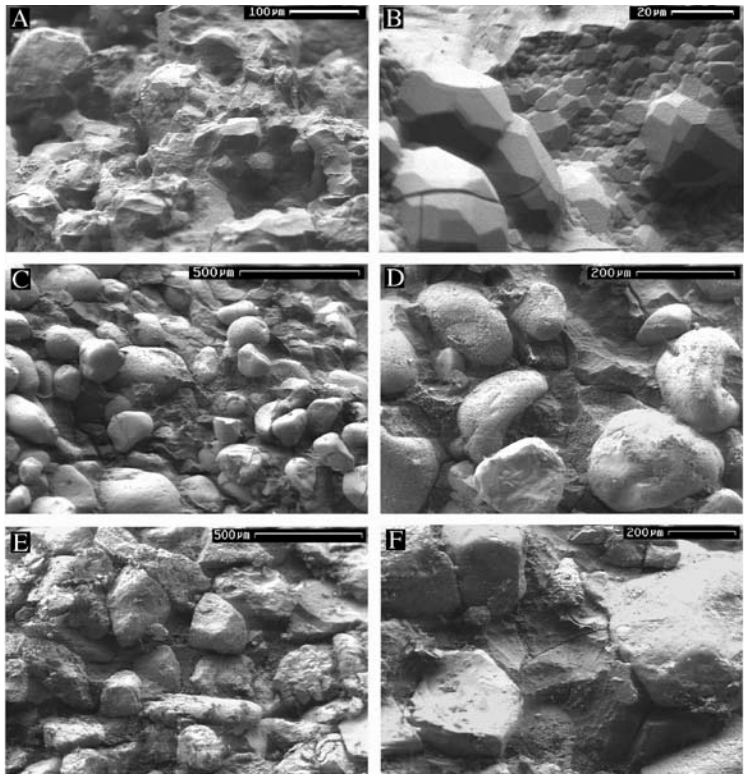

FIGURE 9. Gas hydrate + sediment aggregates. (**a** and **b**) Laboratory-synthesized methane hydrate + quartz sand porous aggregate, formed from quartz grains and seed ice (~50 vol% each) mixed homogeneously prior to reaction. Individual quartz grains are ~100-200 µm. Here, the hydrate coats and loosely cements the quartz particles together, giving the material cohesion. The quartz grains are difficult to distinguish because they are enveloped within hydrate, and the fracture surface tends to propagate through the pore volume of the sample. Several near-surface grains are visible in the top left and bottom left quadrants of (**a**). Faceted grain growth and cubic crystals of methane hydrate (**b**) typically line cavity walls in the as-grown aggregate material. (**c** and **d**) Lab-synthesized methane hydrate + quartz aggregate following hydrostatic compaction and triaxial compression testing at $T > 273$ K. CH_4 pore pressure was maintained on the sample throughout testing to keep the hydrate within its nominal stability field. The sample was then quenched at pressure to 77 K for SEM imaging. This aggregate was made by mixing 50 vol% each quartz sand and granular methane hydrate in a soft metal jacket prior to compaction, and the fresh fracture through the dense material reveals the quartz grains more clearly than in (**a**). The σ_1 compression direction is oriented NE-SW. (**e** and **f**) Natural gas hydrate in nodules recovered from the Mallik drill site, NW Canada. Comparing (**c**) and (**d**) to (**e**) and (**f**) illustrates the striking similarity in phase distribution, grain contacts, and textures that can be achieved by laboratory emulation of as-received natural samples from Arctic permafrost settings.

enhance the rate of recrystallization at earlier stages of synthesis. Of particular note is that hydrate + sand mixtures that were subsequently subjected to full compaction and used in rheological tests showed resulting textures and geometrical arrangement of phases that closely resemble some found in hydrate-bearing samples retrieved from Arctic permafrost (Figs. 9c–f). The advantages of using such synthetic aggregates for material properties testing are that not only are the sample textures easily reproduced or modified in the laboratory, but well-characterized sediment standards can be used for the sediment phase, and the composition and condition of the hydrate can be closely controlled.

Compacted laboratory-synthesized hydrate used in ocean floor experiments

Figure 10 shows the textural development in as-synthesized methane hydrate that underwent full hydrostatic compaction at elevated pressure and temperature above the ice point (panel a), and similarly compacted methane hydrate that was then exposed to a real ocean floor setting (panel b). The latter sample, retrieved after 27 hours from the 1030 m test site (at ~277.5 K), underwent measurable dissolution along its exposed outer surface. The interior of the sample exhibited no apparent evidence of seawater contact, yet as shown in Figure 10b, underwent a remarkable extent of regrowth despite the relatively short duration of the experiment. It remains possible, however, that seawater affected the sample in a visually undetectable manner, or perhaps the improved grain contacts in the fully compacted material aided grain growth. In comparison, "as-synthesized" porous methane hydrate that was also exposed at the seafloor test site underwent substantial dissolution and dissociation in the sample interior throughout the course of the experiment, with water (likely as a dissociation product as well as pore water) being quenched in by liquid nitrogen submersion upon retrieval. The relict morphology of the as-grown material appears to be nonexistent at this final stage (Fig. 10c).

Natural hydrates, and comparison to laboratory-synthesized and annealed hydrates

Figure 11 shows a low-to-high magnification mosaic of textures observed in the interiors of natural gas hydrate nodules collected from the Gulf of Mexico (Core 2569, West Mississippi Canyon site; see also Winters et al. 2004, for further field results). Interpretation of the images remains somewhat uncertain given the many unknowns involving bulk sample composition and the extent of alteration of original textures and/or composition during the recovery process. However, the mosaic gives the general sense of the appearance of the as-received sample texture, material density, pore structure, and pore connectivity.

Without more information for definitive interpretation of morphological features observed in recovered natural gas hydrate samples, our best option at present is to compare the observed textures with those of lab-synthesized samples having well-characterized composition, grain structure, and known pressure-temperature histories. Figure 12 shows both low- and high-resolution features from Gulf of Mexico hydrate (left column) compared to synthetic samples exposed to seafloor conditions (right column). The samples shown in the right-hand column were synthesized as shown in Figure 1, then either compacted as shown in Figure 10 or left uncompacted, then transported under pressure to the ocean floor test site as described above. Those

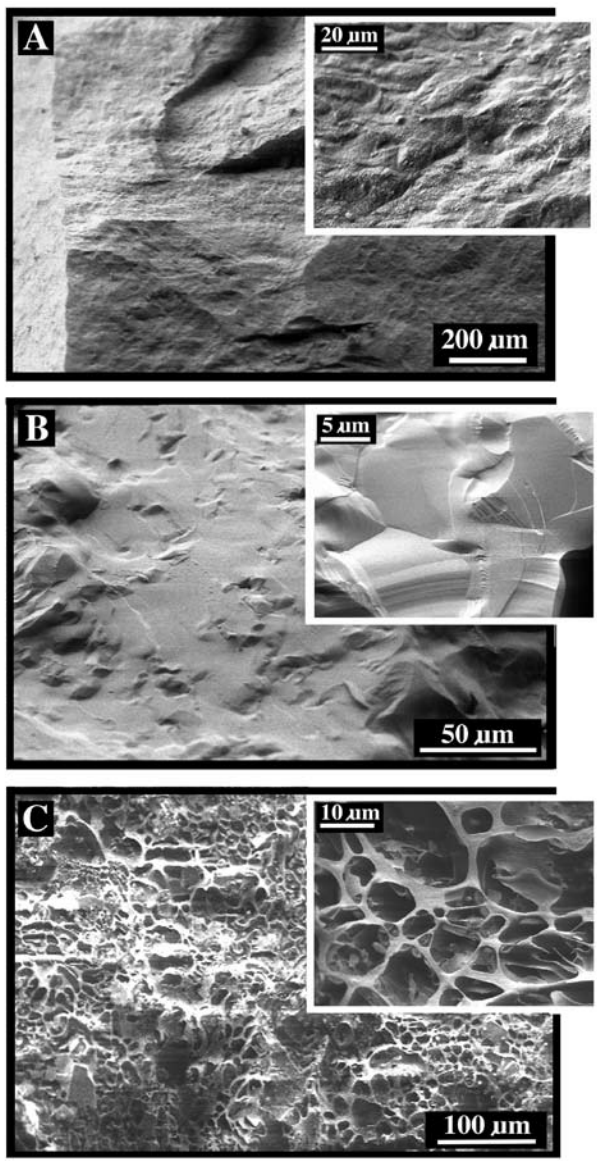

FIGURE 10. Textural development in methane hydrate used for properties testing. (**a**) "As-synthesized" methane hydrate (Fig. 7) that developed fully dense and massive texture after hydrostatic compaction and uniaxial compression at high pressure and >273 K conditions. Confining pressure during compaction was stepped incrementally to 100 MPa while constant pore pressure (~8 MPa CH_4) maintained the hydrate in its equilibrium stability field to 280 K (see also Durham et al. 2003a, 2003b). (**b**) Laboratory-compacted methane hydrate (as shown in **a**) that was then exposed to 1030-meter seafloor conditions, showing that significant annealing takes place after only 27 hours of ocean-floor exposure at ~277 K (see text). (**c**) Porous, "as-grown" methane hydrate that underwent partial dissolution after the same exposure to 1030 m seafloor conditions (see Fig. 12 and text for further discussion). Insets show higher resolution sections of the samples.

samples that did not dissolve after 27 hours were successfully retrieved under pressurized and chilled conditions, and returned to the laboratory for SEM analysis (Stern et al. 2002). The test site was at essentially the same depth from which the Gulf of Mexico core 2569 samples were retrieved, hence offering a basis for comparison.

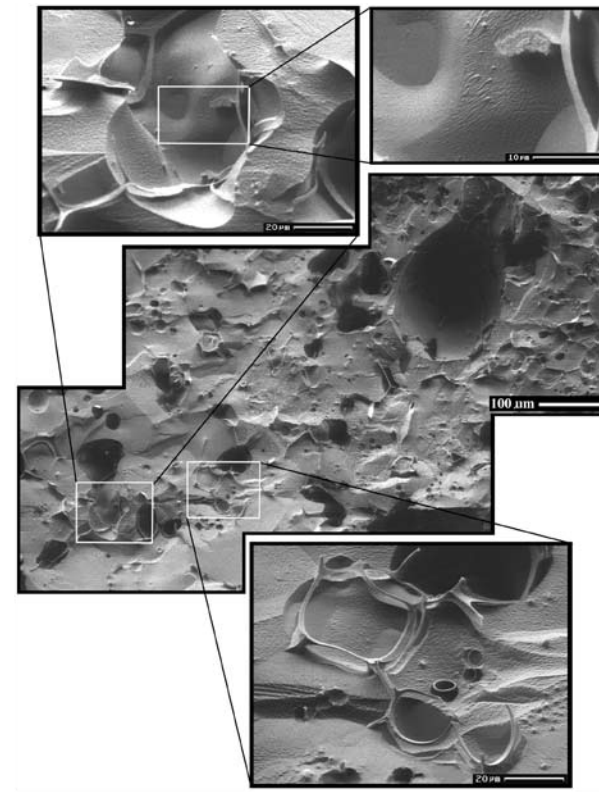

FIGURE 11. Natural sII hydrate from a hydrate-bearing nodule retrieved from the Gulf of Mexico, W. Mississippi Site (after Stern and Kirby 2004). The central mosaic illustrates the general appearance of the hydrate, showing the dense texture of the hydrate material and the general sizes and distribution of the cavities. High resolution enlargements of textural details are shown as cut-away images as marked above and below the mosaic. Other images of these marine hydrates are shown in Figure 12.

Despite the relatively short duration of the ocean-floor experiment, the interiors of both the compacted and uncompacted synthetic hydrates showed surprisingly different grain and pore structure compared to the original as-grown material (compare Fig. 12 to Fig. 7). Even more surprising was the striking similarity in textures and structures displayed by these samples compared to the natural hydrate from core 2569. The highly faceted and finely crystalline grain morphology pervasive in many of our as-grown gas hydrate materials (Figs. 6, 7, 8, 9a, and 9b) is conspicuously absent from all ocean-floor or sub-ocean-floor samples that we have imaged to date. Instead, all natural and synthetic samples retrieved from deep marine conditions developed smooth, minimal-surface-area grain structures, as shown in Figures 10b, 12e, and 12f. Cavity and/or pore geometry also tends to be rounder or more regularly shaped in marine samples than in our "as-synthesized" hydrate, and pores do not appear highly connected in the samples imaged here, except for in near-surface sections of nodules. All seawater-exposed hydrate samples imaged to date exhibit dense hydrate interspersed with micro- to macro-sized pores, with no observed mesoporosity at the intragranular scale.

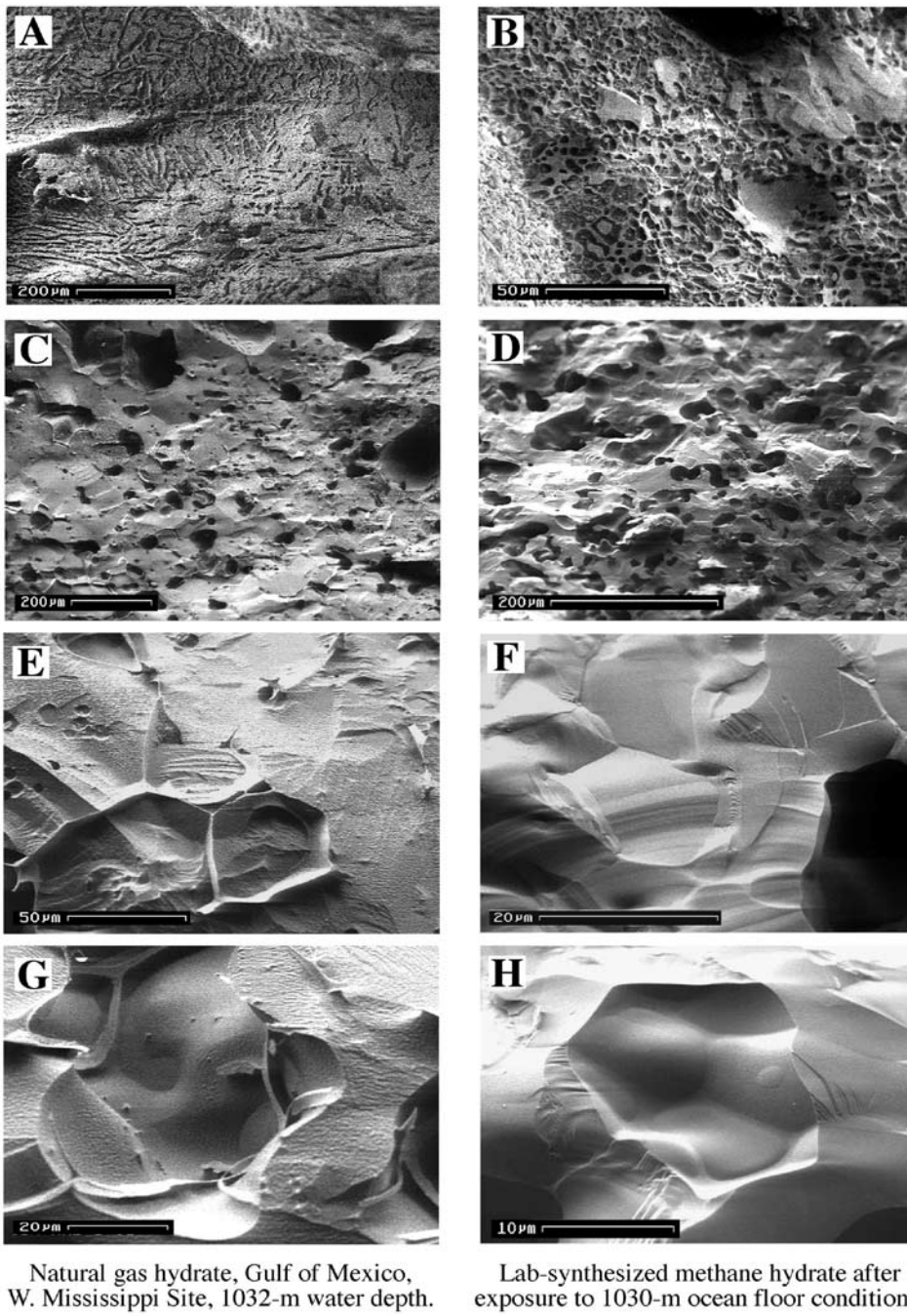

FIGURE 12. Comparison of Gulf of Mexico hydrate (left column) to laboratory-synthesized methane hydrate used in partial dissolution experiments (right column). (**a**) and (**b**) show similarities in grain boundary and pore "cast" textures. (**a**) is from a near-surface section of the natural hydrate, and (**b**) is a 30% porous methane hydrate sample that underwent partial dissolution before subsequent retrieval (see text for further discussion). (**c**) and (**d**) show similar cavity size, distribution, and connectivity in partially compacted sections of samples. (**e**) and (**f**) show similarities in grain size, material density, and clean fracture surfaces. Neither the natural or lab-synthesized material is mesoporous. (**g**) and (**h**) show minimal-surface-area grain textures along cavity walls that we interpret (based on comparison to growth features shown in Figs. 5–7) as grain growth or annealing at the relatively warm seafloor conditions (> 273 K).

DISCUSSION

Ice melting during hydrate synthesis

As described above, our general method of hydrate synthesis involves reacting packed ice grains of 200 μm average grain diameter with the hydrate-forming gas (or liquid) of interest, and pressurizing the system to moderately high pressures. Full and efficient conversion of the ice to hydrate is achieved by then slowly heating the reactants through the ice point and up to temperatures approaching the specific hydrate's *P-T* stability limit. One sustained heating cycle is usually sufficient to completely convert ice to sI methane hydrate, sI CO_2 hydrate, or sII methane-ethane hydrate. In the case of such hydrates as propane hydrate, involving relatively large gas molecules and/or a relatively narrow thermal stability range above the ice point, numerous heating/cooling cycles are required to efficiently convert all the ice to hydrate.

Optical cell observations of methane hydrate synthesis from loosely packed or isolated ice grains indicated that while grain shape integrity is generally maintained throughout reaction, some

recrystallization accompanies early reaction, as evidenced by the development of progressively mottled textures along the surfaces of originally smooth and transparent ice grains (Stern et al. 1998a, 1998b). Based on the pressure-temperature-time records during synthesis, combined with the optical cell investigations, we surmised that while some melting of the ice occurred, the reaction appeared to proceed primarily from the surface inward by diffusion through the outer hydrate layer. The success of the synthesis method appeared to be dependent on those aspects that influenced the availability, transport, and concentration of the hydrate-forming species at the growth front, i.e., those factors that influence diffusion rates, such as high pressure overstep, high temperature, high surface-to-volume ratio of the reacting grains, and small grain size to minimize the volume of the unreacted core. We suggested that such conditions enabled transport of the hydrate-forming gas through the outer hydrate rind and inward to the hydrate/ice interface at a rate sufficiently fast such that incipient melt nuclei react to form gas hydrate faster than they grow to a critical size necessary for bulk melting. Such a process might result in delayed melting, or superheating, of the ice core.

A key assumption underlying this model was that the thin, early formed rinds of hydrate could not act as "pressure seals" around melting cores, masking the pressure signature of bulk melting and the accompanying volume reduction. This assumption, based on earlier predictions that gas hydrates are ice-like in their mechanical properties, we now know to be at least partially incorrect. Our own initial tests on the mechanical strength of methane hydrate (Stern et al. 1996, 1998b) showed that even during compaction and deformation at low-temperature conditions deep within the stability field of methane hydrate, some methane hydrate underwent measurable decomposition to ice, resulting in final samples that contained a significant fraction of ice. The strength of the resulting samples was ice-like, which we interpreted to indicate that the strength of methane hydrate was not significantly different from ice. More recent tests on pure, ice-free methane hydrate samples (Durham et al. 2003a, 2003b), sII methane-ethane hydrate (Durham et al. 2003c), and methane hydrate + quartz sand aggregates (Stern et al. 2004), in which additional procedures were used to expel any free water that developed in samples during compaction, now show that both methane and methane-ethane hydrate are in fact 20 to 100 times stronger than ice.

A second critical factor is the placement of the temperature probe during hydrate synthesis. Thermal indication of ice melting during hydrate synthesis at temperatures above the ice point is clearly visible when thermocouples are placed internally in the sample chamber, in direct contact with the reactants (Fig. 1b). The signature can be greatly masked during external monitoring, however, even when the probe is embedded deep within the wall of the sample chamber. In early methane hydrate synthesis tests, no melt signature was detected by a base-cap-embedded thermocouple upon warming of the reactants through the ice point. In comparison, when the sample chamber was pressurized with ~22 MPa of neon, a non-hydrate-forming gas, the ice grains slowly but completely melted when heated through their melting point, and was clearly detected by the basal thermocouple (Fig. 6b in Stern et al. 1998b). In the former case, the exceptionally low thermal conductivity of methane hydrate (Waite et al. 2002a, 2002b) likely contributed to the poor thermal communication of the sample with the base-cap-embedded probe, as the melting ice and the resulting liquid presumably remained suspended within and between the hydrate encasements.

Based on our current understanding of the exceptionally high strength and low thermal conductivity of methane hydrate relative to ice, we now surmise that these properties can, depending on apparatus configuration, obscure the full *P-T* signature associated with the ice → water phase change during synthesis, a signature (or lack thereof) that formed the basis of superheated ice arguments. The exceptionally high strength of methane hydrate presumably contributes to the commonly observed maintenance of grain shape integrity, such that hydrate-encased liquid maintains particle morphology with only minimal disruption of the outer hydrate shell, despite the volume change associated with the core melting, or despite melt extrusion. We find this quite remarkable given that the thickness of the hydrate "shell" is sometimes less than 10 μm (Fig. 6). We note that our SEM evidence for the apparent melting of cores within intact shells of hydrate are also in general agreement with the NMR and MRM imaging studies by Moudrakovski et al. (1999, 2002). These self-consistent lines of evidence thus indicate that significant melting takes place during hydrate formation from ice at temperatures above the ice point, even in some cases where it is not detected by external monitoring.

A complete understanding of the general reaction still remains somewhat elusive, however. Wang et al. (2002a, b), for example, report neutron diffraction measurements on methane hydrate formation from D_2O ice particles, showing the persistence of ice peaks for nearly 2 hours as sample temperature was increased from 277 to 280 K under ~10 MPa methane pressure. They interpreted their results to be in agreement with our earlier assessment of superheated ice, although they also speculated that the insulating properties of the outer hydrate layer may possibly serve to keep grain-core temperatures lower than those measured in the sample container, and may thus provide a possible alternative explanation for the observed persistence of ice peaks above their melting point.

Within our own samples, another curiosity is that hollow encasements or "shells" of hydrate form in certain sections of many samples (Figs. 6a, 6b, 7c, 7d, and 8), but not ubiquitously throughout all samples. The hollow structures are commonly observed in CO_2 and propane hydrate (Fig. 8), both of which have limited peak synthesis conditions and/or relatively slow rates of reaction. In methane hydrate, the hollow shell structures are typically found in densely packed samples or in dense regions of samples, such as at their base. In the latter case, migration of water from the shell interior is likely augmented by high heat flow through the base of the sample during synthesis (Fig. 1b inset), causing early and rapid melting of the unreacted ice within relatively thin hydrate encasements. The shells also appear to exhibit near-uniform expansion, comparable to that observed previously in optical cell experiments (Stern et al. 1998a, 1998b). Such expansion is expected to occur given the known change in density of molecular water from ice (0.92 g/cm^3) to the hydrate framework (0.78 g/cm^3). Here, in the confines of the reaction vessels, shell surfaces develop into a tightly fitted arrangement with greatly increased grain contact area, while maintaining

near-spherical shapes (Figs. 7c and 7d). It is not clear, however, if expansion and amassing of shells *results* in microfracturing of the encasement, along which melt migrates out, or if the tight configuration is primarily *caused* by late-stage hydrate growth from the relocated melt. Likely a combination of both, given that the nearly isolated grains in optical cell experiments displayed no evidence of melt migration or any significant redistribution of solid material or intergranular pores during standard reaction procedures. In any case, we note that there is no obvious indication of massive deformation or failure of the shell walls in the current experiments, and instead, most all inner-shell exposures are due to the fracturing procedures during SEM sample preparation. The marked emptiness of the shells thus remains quite enigmatic, and the large internal volume of the shells appears somewhat at odds with the volume of material in grain junctions (Figs. 6a, 6b,7c, and 7d). Further experiments are needed to reconcile these seemingly disparate observations and help gain a complete understanding of the reaction process.

Mesoporous growth textures

The partial reaction tests on methane hydrate also reveal the early-stage growth and advancement of highly mesoporous methane hydrate. Formation of such an apparently non-equilibrium texture poses yet another enigmatic process of hydrate formation from melting ice, as the porous microstructure develops at the free-energy cost of hydrate surface energy. This growth texture was first reported by Kuhs et al. (2000) in a variety of gas hydrates grown from ice in the presence of excess gas. Development of the subporous microstructure was investigated further by Salamatin and Kuhs (2002), Staykova et al. (2002, 2003), and Klapproth et al. (2003), all of which provide excellent treatment and quantitative assessment of this growth process and its role and relevance to growth kinetic models at temperatures primarily below the ice point. Mass and heat transfer across a microporous or microperforated hydrate layer has also been discussed in terms of a capillary-permeation model by Mori et al. (1997, 2000).

Possible insight into the occurrence of a porous product may also be gained by drawing analogy with oxidation/corrosion reactions in metals, or with certain mineral replacement reactions (see for example Putnis 2002; Putnis and Pollok 2003). In all of these cases, interconnected porosity in the product should facilitate rapid transport of a mobile reactant (a hydrate-forming gas, a hydrothermal solution, or a corrosive gas or liquid) to the solid reactant, thereby avoiding a slow diffusion pathway through the product. That such reactions can produce porous products also suggests common aspects in the reaction process. In the aqueous solid solution system KBr-KCl investigated by Putnis and Pollok (2003), for example, in which KBr is more soluble than KCl, porous textural development is linked directly to the extent of the volume deficit attending the replacement reaction, and to a lesser extent molar volume reduction. Putnis and Pollok (2003) observed reaction at the crystal/solution interface that advances as a sharp but porous interface, which in turn allows access of the fluid to the solid reactant surface and promotes further reaction. Due to the observed high rate of reaction advancement in the KBr tests (~0.5 μm/s) and the sharpness of the interface, they suggested that the reaction cannot be modeled as diffusion. Similar highly porous replacement textures were also observed in the replacement of leucite by analcime (Putnis et al. 1994; Putnis and Pollok 2003), and microporosity also forms in many feldspars during volume-reduction or mass-transfer processes (Walker et al. 1995). In the case of methane hydrate growth from ice, in which the full reaction ice + gas → hydrate is also volume reducing (despite the volumetric expansion of the H_2O molecular structure), the reaction front is sometimes observed as a sharp front (Fig. 5e), while in other areas it is more irregular (Figs. 5 f, i) or even bulge-like (Figs. 5k,l). These variations suggest that continued gas-ice reactivity to form hydrate at relatively high rates depends on continued gas contact with the ice or water reactant. If local sections of the hydrate product were essentially pore-free, as we know takes place during annealing, the ensuing diffusion-controlled reaction should slow. The more rapid reaction along adjacent porous hydrate areas might then produce such irregularities as those formed during reaction and recrystallization along grain boundaries (Fig. 5).

The shrinking core model

Despite sample-to-sample variability, the similarities between all "as-grown" gas hydrates in this study indicate that the general diffusion-controlled shrinking core model that has been qualitatively discussed by our own group and more quantitatively by others (Henning et al. 2000; Takeya et al. 2000; Moudrakovski et al. 2001; Wang et al. 2002a, 2002b) may not accurately describe sustained growth from ice grains at temperatures above the ice point, even though formation rates may appear in some cases to support such a model. Henning et al. (2000), for example, found that a two-stage shrinking core model can well describe CO_2 hydrate growth from deuterated ice at isothermal conditions below the ice point, as measured by neutron diffraction. Their modeling suggests that the rate-limiting step of the initial stage is the reaction of the hydrate-forming species with the quasi-liquid layer (QLL) or "premelting" layer along exposed surfaces of the ice grains. The limiting process of the latter stage is diffusion of CO_2 through the newly formed surface layer of hydrate. Their findings also suggest that after the hydrate-former diffuses through the outer hydrate layer, subsequent growth proceeds by reaction with internal water in a QLL layer, rather than with ice molecules. Wang et al. (2002a, 2002b) built upon that earlier work to adopt a more complex shrinking core model to fit methane hydrate formation measurements from deuterated ice, at temperatures that cross the ice point. Their model better accounts for spherical surfaces and other reaction steps in addition to diffusion. They reported kinetic measurements that are in agreement with a general diffusion-controlled reaction as the outer hydrate layer grows inward at the expense of the unreacted ice core. They also speculated on the implications of a QLL layer at the ice-core surface. Moudrakovski et al. (2001) adopted a somewhat different approach and provided a thorough treatment of Xe hydrate formation from ice, as measured by NMR at temperatures below the ice point, in terms of the Avrami-Erofeyev kinetic model that describes gas-solid reactions with emphasis on the nucleation stage.

Comparisons of kinetic models are difficult to make, however, given the different techniques and synthesis procedures used by different researchers to investigate specific gas hydrate systems. Of even greater importance is the complexity introduced by the

evolving geometry of samples formed at temperatures above the ice point, due to the considerable migration and redistribution of liquid and solid phases throughout reaction, and by corollary, the absence of grain-for-grain conversion. The porosity and material density changes attending reaction further complicate a quantitative model that unifies both macroscopic and molecular-level measurements. Nevertheless, the textural progression captured here by SEM imaging supports a general reaction model that is consistent both with the results of others on similar key stages of gas hydrate formation from ice (i.e., Kuhs et al. 2000; Staykova et al. 2003; Moudrakovski et al. 1999, 2002, all discussed above) as well as with our own previous measurements. Such reaction appears to involve early hydrate growth as a mesoporous material along ice grain surfaces, followed by hydrate "encasement" development and subsequent core melting as temperatures span the ice point, with significant melt migration occurring in certain compositions and/or configurations of samples, followed by continued redistribution and annealing of material at peak conditions, yielding final development of dense grains of hydrate with faceted crystal growth along free surfaces. Further annealing or other growth processes that continue to develop with ocean-floor exposure also show a consistent trend toward increasingly denser aggregates with greater material density and larger grain size. We have not observed mesoporous hydrates or any faceted crystalline textures in any samples – either lab-synthesized or natural – that were retrieved from ocean floor conditions. Whether mesoporous textures form as original growth textures or persist stably in natural hydrates of permafrost origin thus remains a compelling question for future work.

Implications for further investigations

SEM offers a versatile method for investigating the progress of hydrate-forming reactions and the consequent development of grain and pore structures associated with gas hydrate formation from ice. Here, we document initial growth fronts of highly mesoporous methane hydrate advancing into the dense ice reactant during early reaction from melting ice. Partial-reaction tests show that after ice grain surfaces initially react to produce thin "rinds" of hydrate, the ice cores often melt, with rind microfracturing allowing migration of the melt to adjacent grain boundaries where it also forms hydrate. The development of both the mesoporous texture and the hydrate-encased liquid structures, captured here as transient morphologies that persist primarily, but not exclusively, during the early-to-mid stages of synthesis, are in agreement with previous reports of such structures by others (Kuhs et al. 2000 and Moudrakovski et al. 1999, 2002, respectively). Under the synthesis conditions used in this study, these textures continue to evolve and anneal as reaction reaches completion at peak temperature and pressure conditions, such that the initially mesoporous hydrate anneals to form dense clusters or "domains" of grains. Significant changes in cavity shapes and connectivity also accompany the hydrate growth process, and the relatively simple pore geometry of the initial ice pack develops into a far more complex arrangement in the final as-synthesized material.

SEM serves not only as a powerful tool for characterizing gas hydrates made and/or tested in the laboratory, but also provides an excellent means for elucidating how closely synthetic samples emulate the complexity inherent to natural gas-hydrate-bearing material. Here, we show that methane hydrate + sand aggregates can be synthesized to yield similar textures, phase distribution, and grain contacts as found in some hydrate-bearing materials recovered from permafrost settings. At the other end of the spectrum, even short-term exposure of laboratory-synthesized hydrate to natural ocean-floor conditions can induce extensive textural changes and regrowth of the hydrate. The highly crystalline and fine-grained hydrate formed in the laboratory underwent surprisingly rapid changes, such that the resulting grain and pore structures annealed to closely mimic those observed in natural marine hydrates retrieved from comparable depths. Such regrowth was found to be pervasive even in inner regions of fully dense samples that showed no obvious contact with seawater. This comparison suggests that similar seafloor processes or conditions may have led to similar development of SEM-scale grain structures. On a broader level, these results suggest that investigation of well-characterized synthetic gas hydrate samples that are then exposed to natural settings may serve as a bridge between the controlled laboratory environment and the complexity and change of nature, and may offer a direction with great potential for further developing a more fundamental understanding of gas hydrate growth or recrystallization processes.

As a cautionary note, it can be surprisingly easy to confuse textures arising from different processes without careful testing of the effects of the necessary cryo-preparation and SEM procedures on each specific gas hydrate sample, or without accurate knowledge of a given sample's pressure-temperature history. One outstanding question at this juncture is whether the observed mesoporous growth habit is stable over time, or whether it forms primarily as a nascent texture that eventually anneals to an equilibrium texture. Given that all fully reacted samples that we have examined to-date show extensive and relatively rapid reorganization and densification with time at high temperatures, it seems unlikely that mesoporosity persists stably on the geological timescale. Further comparison of lab-synthesized hydrates with natural hydrates formed from water (marine environments) and ice (permafrost regions) should therefore prove intriguing from a physical chemistry standpoint as well as from mineralogical or geological perspectives. Accurately identifying in situ growth features and distinguishing them from features produced as artifacts of the recovery or processing methods will likely remain challenging in at least the near future, as will be the unequivocal distinction between mesoporous growth textures and low-temperature dissociation features in samples with even partially unknown formation or processing histories.

Acknowledgments

Funding was provided in part by the USGS Gas Hydrate Project, the Methane Hydrate R&D Program of the U.S. Dept. of Energy (National Energy and Technology Laboratory), and NASA's Planetary Geology and Geophysics Program. We thank S. Dallimore of the Canadian Geological Survey for providing the samples shown in Figures 9e and f. Samples from ocean-floor dissolution tests described in the text and shown in Figures 12b, d, f, and h were obtained in collaboration with Monterey Bay Aquarium Research Institute scientists P. Brewer and E. Peltzer. We thank W. Waite, I-Ming Chou (both USGS), and two anonymous reviewers for helpful reviews of the manuscript, and R. Oscarson and J. Pinkston (USGS) for their technical assistance. Part of this work was performed under the auspices of the U.S. Department of Energy by the Lawrence Livermore National Laboratory under contract W-7405-ENG-48. We also thank Bryan Chakoumakos for his editorial help with this paper.

REFERENCES CITED

Circone, S., Kirby, S.H., Pinkston, J.P., and Stern, L.A. (2001) Measurement of gas yields and flow rates using a custom flow meter. Review of Scientific Instruments, 72, 2709–2716.

Circone, S., Stern, L., Kirby, S., Durham, W., Chakoumakos, B.C., Rawn, C.J., Rondinone, A.J., and Ishii, Y. (2003) CO_2 hydrate: synthesis, composition, dissociation behavior, and a comparison to structure I CH_4 hydrate. Journal of Physical Chemistry B, 107, 5529–5539.

Circone, S., Stern, L.A., and Kirby, S.H. (2004) The role of elevated methane pressure on methane hydrate dissociation rates. American Mineralogist, 89, 1192.

Dallimore, S.R. and Collett, T.S., Eds. (2004) Scientific Results from the Mallik 2002 Gas Hydrate Production Research Well Program, Mackenzie Delta, Northwest Territories, Canada. Geological Survey of Canada, Bulletin 585, in press.

Durham, W.B., Kirby, S.H., Stern, L.A., and Zang, W. (2003a) The strength and rheology of methane clathrate hydrate. Journal of Geophysical Research, 108, 2182–2193.

Durham, W.B., Stern, L.A., and Kirby, S.H. (2003b) Ductile flow of methane hydrate. Canadian Journal of Physics, 81, 373–380.

Durham, W.B., McDaniel, S., Stern, L.A., and Kirby, S.H. (2003c) Ice rheology in the planetary context. European Geophysical Society, Geophysical Research Abstracts, 5, 12592.

Freifeld, B.M., Kneafsey, T.J., Tomutsa, L., Stern, L.A., and Kirby, S.H. (2002) Use of computed x-ray tomographic data for analyzing the thermodynamics of a dissociating porous sand/hydrate mixture. Proceedings of the 4th International Conference on Gas Hydrates, Yokohama, Japan, 750–755.

Helgerud, M.B., Waite, W.F., Kirby, S.H., and Nur, A. (2003) Measured temperature and pressure dependence of Vp and Vs in compacted, polycrystalline sI methane and sII methane-ethane hydrate. Canadian Journal of Physics, 81, 47–53.

Henning, R.W., Schultz, A.J., Thieu, V., and Halpern, Y. (2000) Neutron diffraction studies of CO_2 clathrate hydrate: formation from deuterated ice. Journal of Physical Chemistry A, 104, 5066–5071.

Klapproth, A., Goreshnic, E., Staykova, D., Klein, H., and Kuhs, W. (2003) Structural studies of gas hydrates. Canadian Journal of Physics, 81, 503–518.

Kuhs, W., Klapproth, A., Gotthardt, F., Techmer, K., and Heinrichs, T. (2000) The formation of meso- and macroporous gas hydrates. Geophysical Research Letters, 27, 2929–2932.

Makogon, Y. (1997) Hydrates of Hydrocarbons, 482 p. PennWell Publishing Co., Tulsa, Oklahoma.

Mikami, J., Masuda, Y., Ushida, T., Satoh, T., and Takeda, H. (2000) Dissociation of natural gas hydrate observed by X-ray CT scanner. In G.D. Holder and P.R. Bishnoi, Eds., Gas Hydrates, Challenges for the Future. Annals of the New York Academy of Science, 912, 1011–1020.

Mori, Y.H. and Mochizuki, T. (1997) Mass transport across clathrate hydrate films – a capillary permeation model. Chemical Engineering Science, 52, 3613–3616.

——— (2000) Modeling of simultaneous heat and mass transfer to/from can across a hydrate film. Annals of the New York Academy of Sciences, 912, 633–641.

Mork, M., Schei, G., and Larsen, R. (2000) NMR imaging study of hydrates in sediments. In G.D. Holder and P.R. Bishnoi, Eds., Gas Hydrates, Challenges for the Future. Annals of the New York Academy of Science, 912, 897–905.

Moudrakovski, I.L., Ratcliffe, C.I., McLaurin, G.E., Simard, B., and Ripmeester, J.A. (1999) Hydrate layers on ice particles and superheated ice: a ^1H NMR microimaging study. Journal of Physical Chemistry A, 103, 4969–4972.

Moudrakovski, I.L., Sanchez, A., Ratcliffe, C.I., and Ripmeester, J.A. (2001) Nucleation and growth of hydrates on ice surfaces: new insights from 129 Xe NMR experiments with hyperpolarized xenon. Journal of Physical Chemistry B, 105, 12338–12347.

Moudrakovski, I.L., Ratcliffe, C.I., and Ripmeester, J.A. (2002) Application of Magnetic Resonance Microimaging (MRM) to monitor the formation of gas hydrate. Proceedings of the 4th International Conference on Gas Hydrates, Yokohama, Japan, 444–448.

Putnis, A. (2002) Mineral replacement reactions: from macroscopic observations to microscopic mechanisms. Mineralogical Magazine, 66, 689–708.

Putnis, C.V. and Pollok, K. (2003) Porous mineral textures as indicators of the mechanism of replacement reactions. European Journal of Mineralogy, 15, 153.

Putnis, A., Putnis, C., and Giampaolo, C. (1994) The microtexture of analcime phenocrysts in igneous rocks. European Journal of Mineralogy, 6, 627–632.

Rawn, C.J., Rondinone, A.J., Chakoumakos, B.C., Marshal, S.L., Stern, L.A., Circone, S., Kirby, S.H., Jones, C.Y., Toby, B.H., and Ishii, Y. (2002) Neutron powder diffraction studies as a function of temperature of structure II hydrate formed from a methane + ethane gas mixture. Proceedings of the 4th International Conference on Gas Hydrates, Yokohama, Japan, 595–603.

Rawn, C.J., Rondinone, A.J., Chakoumakos, B.C., Circone, S. Stern, L.A., Kirby, S.H., and Ishii, Y. (2003) Neutron powder diffraction studies as a function of temperature of structure II hydrate formed from propane. Canadian Journal of Physics, 81, 431–438.

Rehder, G., Kirby, S., Durham, W., Stern, L., Peltzer, E.T., Pinkston, J., and Brewer, P. (2004) Dissolution rates of pure methane hydrate and carbon dioxide hydrate in undersaturated seawater at 1000 m depth. Geochimica Cosmochimica Acta, 68, 285–292.

Salamatin, A.N. and Kuhs, W.F. (2002) Formation of porous gas hydrates. Proceedings of the 4th International Conference on Gas Hydrates 2002, 766–770.

Sloan, E.D. Jr. (1998) Clathrate Hydrates of Natural Gases (revised edition), 705 p. Marcel Dekker, Inc., New York, Basel.

Smelik, E.A. and King, H.E. Jr. (1997) Crystal-growth studies of natural gas clathrate hydrates using a pressurized optical cell. American Mineralogist, 82, 88–98.

Staykova, D.K., Hansen, T., Salamatin, A.N., and Kuhs, W.F. (2002) Kinetic diffraction experiments on the formation of porous gas hydrate. Proceedings of the 4th International Conference on Gas Hydrates, Yokohama, Japan, 537–542.

Staykova, D.K., Kuhs, W.F., Salamatin, A.N., and Hansen, T. (2003) Formation of porous gas hydrate from ice powders: diffraction experiments and multi-stage model. Journal of Physical Chemistry B, 107, 10299–10311.

Stern, L.A. and Kirby, S.H. (2004) Grain and pore structure imaging of gas hydrate from core MD02-2569 (West Mississippi Site, Gulf of Mexico): a first look by SEM. In W. Winters, Ed., Initial Report on Gas Hydrate and Paleoclimate Results from the RSV Marion-Dufresne Cruise to the Gulf of Mexico July 2002. U.S. Geological Survey Digital Data Series Publications, in press.

Stern, L., Kirby, S., and Durham, W. (1996) Peculiarities of methane clathrate hydrate formation and solid-state deformation, including possible superheating of water ice. Science, 273, 1843–1848.

Stern, L.A., Hogenboom, D.L., Durham, W.B., Kirby, S.H., and Chou, I-M. (1998a) Optical cell evidence for superheated ice under gas-hydrate-forming conditions. Journal of Physical Chemistry B, 102, 2627–2632.

Stern, L.A., Kirby, S.H., and Durham, W.B. (1998b) Polycrystalline methane hydrate: synthesis from superheated ice, and low-temperature mechanical properties. Energy and Fuels, 12, 201–211.

Stern, L., Kirby, S., Durham, W., Circone, S., and Waite. W. (2000) Synthesis of pure methane hydrate suitable for measurement of physical properties and decomposition behavior. In M.D. Max, Ed., Natural Gas Hydrate: In Oceanic and Polar Subaerial Environments, Chapter 25, p. 323–349. Kluwer, Dordrecht.

Stern, L., Peltzer, E., Durham, W., Kirby, S., Brewer, P., Circone, S., and Rehder, G. (2002) Dissolution of hydrocarbon gas hydrates in seawater at 1030 meters; effects of porosity, structure, and compositional variation as determined by high-definition video and SEM imaging. EOS, Transactions of the American Geophysical Union, 83, abstract OS21B-0216, F777.

Stern, L., Circone, S., Kirby, S., and Durham, W. (2003) Temperature, pressure, and compositional effects on anomalous or "self" preservation of gas hydrates. Canadian Journal of Physics, 81, 271–283.

Stern, L.A., Durham, W.B., Kirby, S.H., Circone, S., and Helgerud, M.B. (2004) Experimental observations pertinent to the mechanical and thermal stability of sI methane hydrate/sand aggregates. Extended abstract, American Association of Petroleum Geologists Annual Meeting 2004, Dallas, Texas.

Suess, E., Borhmann, G., Rickert, D., Kuhs, W.F., Torres, M.E., Trehu, A., and Linke, P. (2002) Properties and fabric of near-surface methane hydrates at Hydrate Ridge, Cascadia Margin. Proceedings of the 4th International Conference on Gas Hydrates, Yokohama, Japan, 740–744.

Takeya, S., Hondoh, T., and Uchida, T. (2000) In situ observation of CO_2 hydrate by X-ray diffraction. In G.D. Holder and P.R. Bishnoi, Eds., Gas Hydrates, Challenges for the Future. Annals of the New York Academy of Science, 912, 973–982.

Uchida, T., Dallimore, S., and Mikami, J. (2000) Occurrences of natural gas hydrates beneath the permafrost zone in Mackenzie Delta, Visual and X-ray CT Imagery, In G.D. Holder and P.R. Bishnoi, Eds., Gas hydrates, Challenges for the Future. Annals of the New York Academy of Science, 912, 1021–1033.

Waite, W.F., Pinkston, J.P., and Kirby, S.H. (2002a) Preliminary laboratory thermal conductivity measurements in pure methane hydrate and methane hydrate-sediment mixtures: a progress report. Proceedings of the 4th International Conference on Gas Hydrates, Yokohama Japan, 728–733.

Waite, W., deMartin, B., Pinkston, J., Kirby, S., and Ruppel, C. (2002b) Thermal conductivity measurements in porous mixtures of methane hydrate and quartz sand. Geophysical Research Letters, 29, 2229, doi:10.1029/2002GL015988.

Walker, F.D.L., Lee, M.R., and Parsons, I. (1995) Micropores and micropermeable texture in alkali feldspars: geochemical and geophysical implications. Mineralogical Magazine, 59, 505–534.

Wang, X., Schultz, A.J., and Halpern, Y. (2002a) Kinetics of ice particle conversion to methane hydrate. Proceedings of the 4th International Conference on Gas Hydrates, Yokohama, Japan, 455–460.

——— (2002b) Kinetics of methane hydrate formation from polycrystalline deuterated ice. Journal of Physical Chemistry A, 106, 7304–7309.

Winters, W., Lorenson, T., and Paull, C., Eds. (2004) Initial Report on Gas Hydrate and Paleoclimate Results from the RSV Marion-Dufresne Cruise to the Gulf of Mexico July 2–18, 2002. U.S. Geological Survey Digital Data Series Publication, in press.

MANUSCRIPT RECEIVED OCTOBER 28, 2003
MANUSCRIPT ACCEPTED APRIL 25, 2004
MANUSCRIPT HANDLED BY BRYAN CHAKOUMAKOS